Nigerian Journal of Technology (NIJOTECH)
Vol. 43, No. 3, September, 2024, pp.509 - 517
www.nijotech.com

Print ISSN: 0331-8443
Electronic ISSN: 2467-8821
https://doi.org/10.4314/njt.v43i3.13

A SYNTHETIC PID GAIN TUNING FRAMEWORK FOR ROBUST PITCH ATTITUDE CONTROL OF SLENDER AIRFRAMES

AUTHORS:
T. A. Fashanu[1,*], L. M. Adetoro[2], A. A. Ayorinde[3], O. S. Asaolu[4] and M. A. Ogundero[5]

AFFILIATIONS:
[1,4,5]Department of Systems Engineering, University of Lagos, Nigeria.
[2]National Agency for Space Research and Development, FCT Abuja, Nigeria.
[3]Department of Electrical and Electronics Engineering, University of Lagos, Nigeria.

***CORRESPONDING AUTHOR:**
Email: tfashanu@unilag.edu.ng

ARTICLE HISTORY:
Received: 12 May, 2023.
Revised: 06 June, 2024.
Accepted: 28 August, 2024.
Published: 20 September, 2024.

KEYWORDS:
Airframe Vibrations, Algorithm Development, PID Gains Auto-tuning, Hybrid Simulation Rig, Slender Microsatellite Launch Vehicles.

ARTICLE INCLUDES:
Peer review

DATA AVAILABILITY:
On request from author(s)

EDITORS:
Ozoemena Anthony Ani

FUNDING:
None

Abstract

The need to decentralize microsatellite launch missions, as a result of rapid expansion of space technology has led to the emergence of slender (microsatellite) launch vehicles (SLV). However, navigation cost, in terms of onboard equipment, state estimation and control algorithms presently prohibits microsatellite launch vehicle missions. Thus, to realize mission affordability of slender launch vehicles, this work developed a Hardware In the Loop rig for optimizing hardware cost and maximizing the performance of implemented state estimation and control algorithms on slender launch vehicles navigation systems. Apriori, the National Agency for Space Research and Development Agency scaled the characteristics of NASA's Ares I Rocket launcher to obtain a miniaturized slender launch vehicle. This prototype is interfaced with MATLAB's SIMULIINK environment to build an experimental rig for autopilot simulation to realize affordable navigation systems on slender launch vehicles. In the feedback control loop of the simulated autopilot system, the proportional, integral and derivative control gains of the simulated autopilot were initialized by classical control laws; this seamlessly transits to a smart fuzzy logic based gain selection algorithm within the rise time of the system's response. This smartly filters nonlinear structural vibration noise from the state estimation system, as well as proactively selects the proportional, integral and derivative gains of the autopilot system. Inference from the flight data sheet established rigorous coupling between structural and control hardware dynamics. Thus, to demonstrate structural interference cancellation, and improve on the auto-tuning ability of the semi- intelligent pitch attitude control algorithm; a pre-planned rocket trajectory of 700m altitude and 15 seconds flight duration was modelled for adaptive tracking such that the desired control objectives are realised. In profile, the realized trajectory indicated that dynamic interaction between rocket structure and control hardware was effectively attenuated. In-flight, the recorded maximum deviation from the referenced trajectory is 0.16% (overshoot). This transient error is mostly due to unmodelled wind induced structural excitation.

1.0 INTRODUCTION

Traditionally, microsatellites and other lightweight space bound payloads are aggregated for a conventional space mission. With Rapid development in space technology, more frequent space missions are now required. This has led to the development of dedicated slender (microsatellite) launch vehicles (SLV). Meanwhile, due to non-linear structural vibrations resulting from very high aspect ratio and bending modes, navigation of SLVs are more complicated than of the conventional launchers. Even for these heavy launchers, the navigation system accounts for over

HOW TO CITE:
Fashanu, T. A., Adetoro, L. M., Ayorinde, A. A., Asaolu, O. S., and Ogundero, M. A. "A Synthetic Gain Selection Framework for Robust Pitch Attitude Control of Slender Airframes", *Nigerian Journal of Technology*, 2024; 43(3), pp. 509 – 517; *https://doi.org/10.4314/njt.v43i3.13*

65% of the launching cost [1] because it consists of high fidelity hardware and high-end computational algorithms. Such hardware is mostly available on specialised demands at prohib-itive costs. As such, it is important that aerospace vehicles for dedicated missions should be more cost effective. It is in this regard that this work addressed the possibility of using affordable off-the-shelf hardware with intelligent control algorithms to synthesise robust and cost effective navigation systems for dedicated slender launch vehicles.

To resolve the issues outlined above, primarily, it is necessary to experimentally simulate nonlinear effects of structural vibrations, time delays, resonance and control loop bandwidth on the time response of SLV autopilot systems. These extraneous factors complicate the dynamics of slender aerospace vehicles [2]. Consequently, special attention is paid to resolve them in the control loop. In earlier works, this is done by selecting high-end hardware, deployment of high fidelity filters and high precision computational algorithms. In addition to the factors stated earlier, the control response of SLVs autopilots are further compounded by bending modes, fuel sloshing, uncertain aerodynamics and engine gimbal [3]. Meanwhile, bending mode control and its related dynamics has been increasingly studied and advanced for flexible launch vehicles that are modelled as Euler-Bernoulli beams [4] [5] [6]. Similarly, control algorithm development, analyses of equations of motion, as well as the stability and control of dedicated launch vehicles that are idealized as rigid body systems have also been investigated by various authors using different dynamic models [7].

The rigid airframe structural approach facilitates closed form analytical solutions. It oversimplifies the analysis of systems response by expressing it in terms of finite and well-known functions. These response analyses have supported the navigation of heavy space vehicles. However, it has limited applications on SLVs. Clearly, beyond a certain limit of airframe aspect ratio; for accurate simulation, design and synthesis of a robust pitch attitude control systems, detailed vibration analysis of the bending modes and other system's nonlinearities must be considered for effective navigation [8]. This is required for precision tracking of the pitch attitude and rocket trajectory in the presence of bending modes, dynamics and other non-linearities. Unlike the case of heavy launchers, this nonlinear vibration and bending mode problem defies closed form analytical solutions.

Consequently, the reliability of the pitch attitude control system of SLVs depends on high precision state estimation of displacement, rate of rotation and acceleration at every point on the vehicle. Otherwise, mission planning and pitch attitude control system design would be significantly compromised [9]. For this purpose, [10] investigated the complex problem of including the effect of bending modes on Ares-1 Launch Vehicle. In all, the precision and reliability of an autopilot-controlled flexible rocket critically depend on accurate representation of the vehicle's elastic motion under the prevailing in-flight forces and the reliability of its state filters. Thus, this paper attempts to synthesize a robust control system for navigating airframes in the presence of structural vibration.

2.0 FLEXIBLE AIRFRAME DYNAMICS AND IN-FLIGHT INSTRUMENTATION PATHOLOGIES

Beyond the quality of state sensors and the computational accuracy of the state estimation algorithm, the relative positions of state sensors on the airframe also determine the performance of the autopilot feedback control loops of the vehicle [11]. Thus, with appropriate sensor placement on the slender airframe in a way that minimizes the effects of the bending modes of the structure, affordable sensors can be deployed for feasible microsatellite launch missions [12].

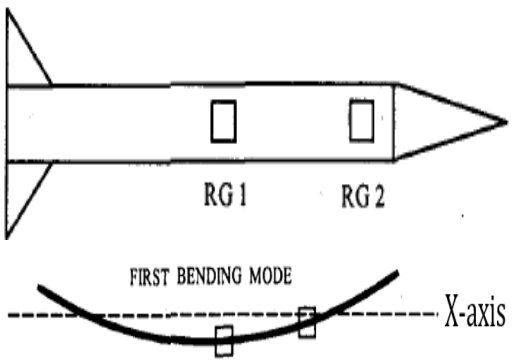

Figure 1: Sensors and actuator placement on slender airframes relative to bending modes [Source: 13]

Details of the performance of state measuring devices, as determined by the choice of control sensors, their arrangement on airframe structure and their impact on the precision of pitch attitude control loop decisions was reported by [14]. Precisely, some strategic position of state sensors are known to significantly filter influence of elastic oscillations on the measured parameters of vehicle motion [15]. In this regard, the

general guideline is to place the rate gyros and angle sensors near the anti-nodes of the first node of structural deflections, while the accelerometers are positioned at the nodes. With this approach, the sensors sense the least noisy signal due to flexible modes. This is illustrated in Figure 1.

Theoretically, optimum sensor locations are the nodes and antinodes of the air frames structural oscillations. However, in design they may coincide with joints and couplers positions. Hence, in practice, these locations may be inaccessible [15] [16]. As a result, in the elastic beam models, nonlinear system's phenomena such as the natural frequencies, mode shapes, and the damping factors at the design stage often lead to inexact system's parameters; due to imprecise placement of sensors and actuators [17]. Consequently, in-flight; high resolution real time state estimation and filtering algorithms are required to compensate for instrumentation and parametric errors [18]. To date, to the best of our knowledge, pitch attitude control loop design that is based on real-time correction of error that is introduced to the instrumentation data by airframe bending is fully developed; This is the basis for this work.

3.0 COMPUTATIONAL FRAMEWORK FOR PITCH ATTITUDE CONTROL OF NON RIGID ROCKET

As a starting point, we present the mathematical model of the pitch plane motion of a flexible launch vehicle shown in Figure 2 for the purpose of control algorithm and hardware in the loop development.

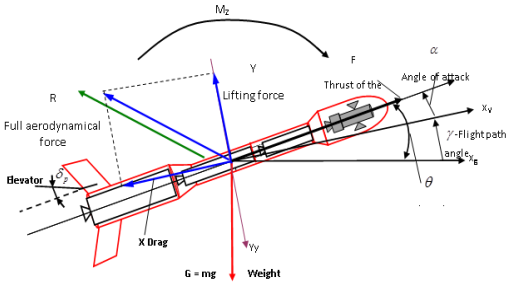

Figure 2: Pitch plane motion of rocket

To define non rigid longitudinal plane of the rocket, it is idealized as a slender elastic rod of length L with a mass density function $m(x,t)$ and flexural stiffness *EJ(x)*. Thus, the corresponding equation of lateral vibrations of such rocket in a longitudinal plane is presented by [10] as:

$$\frac{\partial^2}{\partial x^2}\left(E(x)J(x)\frac{\partial^2 q(x,t)}{\partial x^2}\right)+m(x,t)\frac{\partial^2 q(x,t)}{\partial x^2}=f(x,t) \quad (1)$$

where $E(x)$ is modulus of elasticity; $J(x)$ is moment of inertia of cross-sectional area of a rod and *f*(x,t) is external distributed load.

To analyse the dynamics of the rocket in the context of measurement and instrumentation for the design of its pitch attitude control system; the solution of Equation (1) is sought with attention to the mass and deflection of the rod through the mode shape function $\varphi(x)$, modal coordinates $\xi(t)$ and bending mode frequency ω such that;

$$q(x,t)=\varphi(x)\xi(t) \quad (2)$$

In terms of Equation (2); in its homogeneous form, Equation (1) transforms to;

$$E(x)J(x)\varphi^4(x)+m(x)\omega^2\varphi(x)=0 \quad (3)$$

Thus, the corresponding second order deflection dynamics is expressed as;

$$\ddot{\xi}(t)+\omega^2\xi(t)=0 \quad (4)$$

For a simplified free-free rod model, the initial and boundary conditions are presented respectively as:

$$q|_{t=0}=q(x,0),\frac{\partial q}{\partial t}|_{t=0}=q(x,0);$$
$$E(x)I\frac{\partial^2 q}{\partial x^2}|_{x=0,x=l}=0,\frac{\partial}{\partial x}\left(E(x)I\frac{\partial^2 q}{\partial x^2}\right)|_{x=0,x=l}=0 \quad (5)$$

Meanwhile, the modes of natural oscillations of an elastic rocket for different orthogonal bending mode frequencies on a section [0, L] are given as:

$$\int_0^L \varphi_i(x)\varphi_j(x)M(x)dx=0;\ i=j. \quad (6)$$

$$\int_0^L \varphi_i(x)\varphi_j(x)m(x)dx=0;i\neq j. \quad (7)$$

Given the definitions in Equations (6 and 7), the forced oscillation of the rocket is thus determined by the following system of ordinary differential equations;

$$M_i\ddot{\xi}_i+M_i\omega_i^2\xi_i=\Xi_i;\ (i=1,2,\ldots\infty); \quad (8)$$

$$M_i=\int_0^L \varphi_i m(x)dx;\ \Xi_i=\int_0^L \varphi_i f(x,t)dx; \quad (9)$$

where $\ddot{\xi}_i$ are the generalized coordinates. Similarly, M_i and Ξ_i are the generalized mass and force.

Consequently, considering the first two bending mode frequencies and corresponding damping effects, the pitch plane angular and translational motion of an elastic airframe takes the form;

$$m_0V(\dot{\vartheta}-\dot{\alpha})=Y; \quad (10)$$

In Equation 10, Y is torque exerted on the rocket in axial direction by applied external forces.

$$J\ddot{\vartheta}=M_{Z1}; \quad (11)$$

Thus for the first bending mode we have;

$$M_1(\ddot{\xi}_1+2\zeta_1\omega_1\dot{\xi}_1+\omega_1\dot{\xi}_1)=\Xi_1; \quad (12)$$

Similarly, the deflection dynamics of the second bending mode is expressible as;

$$M_2(\ddot{\xi}_2+2\zeta_2\omega_2\dot{\xi}_2+\omega_2\dot{\xi}_2)=\Xi_2; \quad (13)$$

where $\dot{\vartheta}$ is the first derivative of pitch angle, $\ddot{\vartheta}$ is its second derivative, $\dot{\alpha}$ is rate of change of angle of attack, M_{Z1} is pitch angle moment, m_0 its mass and V represents its velocity. Subscripts 1 and 2 denote the 1st and 2nd bending mode parameters of damping

coefficients ζ_1 ,ζ_2; modal coordinates $\dot{\xi}_1$, $\dot{\xi}_2$, and frequencies ω_1, ω_2.

3.1 Hybrid In-Flight Controller and Flexible Airframe Stabilization Measures

Given that the launch vehicles are programmed to follow pre-planned trajectories. Their autopilots are essentially Model Reference Adaptive Control systems. For this purpose, we consider a feedback control loop with Proportional, Integral and Derivative (PID) gains (i.e. K_p, K_i and K_d) that are tuned in real time using fuzzy logic rules. This smart controller has two inputs-three outputs so that it adjusts the control parameters according to changing operation and deviations from the reference trajectory. The overall scheme is as shown in Figure 3.

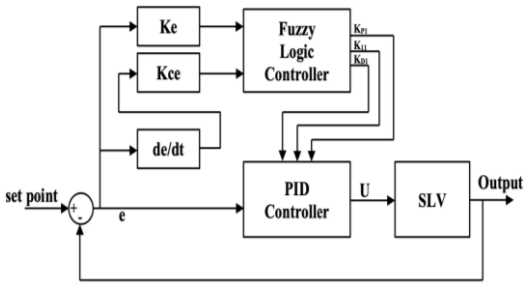

Figure 3: Dynamic control gains-fuzzy tuned PID system

As stated above, the PID parameters are tuned using fuzzy inference engine. This provides a nonlinear mapping of the error and derivative of error to PID parameters. The fuzzy system is constructed from a set of fuzzy IF-THEN rules that describe how to choose the PID gains under certain operational conditions. To streamline decision making, the gains K_p and K_d are normalized to the range between zero and one by the following linear transformation:

$$\alpha = T_i/T_d \quad (14)$$

Where T_i is integral time constant and T_d is derivative time constant:

$$T_i = \frac{K_p}{K_i};\ T_d = \frac{K_d}{K_p} \quad (15)$$

This leads to

$$K_i = \frac{K_p}{(\alpha T_d)} = K_p^2/(\alpha K_d) \quad (16)$$

The ranges $[K_{p\,min}, K_{p\,max}] \subset R$ and $[K_{d\,min}, K_{d\,max}] \subset R$ are structured such that the proportional gain $K_p \in [K_{p\,min}, K_{p\,max}]$ and the derivative gain $K_d \in [K_{d\,min}, K_{d\,max}]$ are bounded, such that normalized gains K_p and K_d are;

$$K_p' = \frac{K_p - K_{p\,min}}{K_{p\,max} - K_{p\,min}} \quad (17)$$

$$K_d' = \frac{K_d - K_{p\,min}}{K_{d\,max} - K_{d\,min}} \quad (18)$$

Hence,

$$K_p \in [K_{p\,min}, K_{p\,max}] \text{ and } K_d \in [K_{d\,min}, K_{d\,max}] \quad (19)$$

The above considerations lead to set of neuro fuzzy IF-THEN rules for adjusting error, error rate as well as the gains K_p, K_d and α in the fuzzified membership function given by Figure 4; in which, NB is Negative Big, NS is Negative Small, NM is Negative Medium, PB is Positive Big, PS is Positive Small, ZO is Zero, S is Small, B is Big and M is Medium in the membership functions.

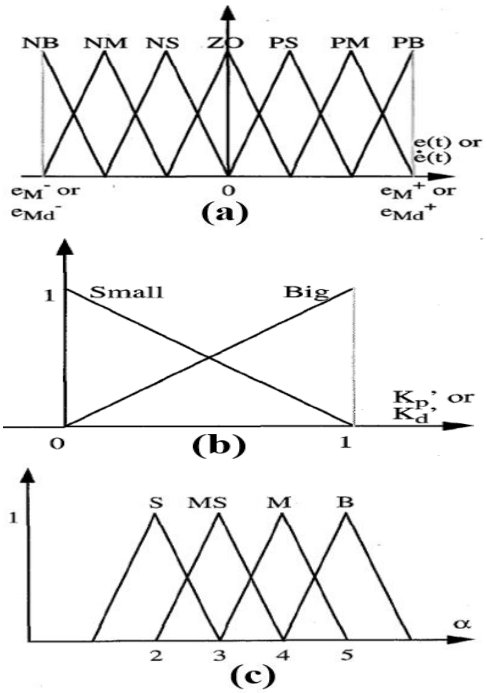

Figure 4: (a) Membership function error (b) Membership function Kp: (c) Membership function K_d

Appropriate PID control gains were therefore tuned on a real time basis using IF-THEN rules of fuzzy logic in the following forms:

(a)		ė(t)						
		NB	NM	NS	ZO	PS	PM	PB
e(t)	NB	B	B	B	B	B	B	B
	NM	S	B	B	B	B	B	S
	NS	S	S	B	B	B	S	S
	ZO	S	S	S	B	S	S	S
	PS	S	S	B	B	B	S	S
	PM	S	B	B	B	B	B	S
	PB	B	B	B	B	B	B	B

(b)		ė(t)						
		NB	NM	NS	ZO	PS	PM	PB
e(t)	NB	S	S	S	S	S	S	S
	NM	B	B	S	S	S	B	B
	NS	B	B	B	S	B	B	B
	ZO	B	B	B	B	B	B	B
	PS	B	B	B	S	B	B	B
	PM	B	B	S	S	S	B	B
	PB	S	S	S	S	S	S	S

(c)		ė(t)						
		NB	NM	NS	ZO	PS	PM	PB
e(t)	NB	2	2	2	2	2	2	2
	NM	3	3	2	2	2	3	3
	NS	4	3	3	2	3	3	4
	ZO	5	4	3	3	3	4	5
	PS	4	3	3	2	3	3	4
	PM	3	3	2	2	2	3	3
	PB	2	2	2	2	2	2	2

Figure 5: (a) Fuzzy tuning rules for K_p (b) Fuzzy tuning rules for K_d (c) Fuzzy tuning rules for α.

Forty Nine rules were combined in each membership set using product inference engine, singleton fuzzifier, and center average defuzzifier in MATLAB; that is, the parameters K_p, K_d, and α are tuned on-line according to rules defined in Figure 5. To ensure a high level of performance throughout the flight duration. The smart PID control gains ensure that, if the desired outputs are smaller than the reference model, then the smart gain selection machine proportionally increases the forward loop gain. Conversely, when the error signals become large, signaling the onset of instability, the forward loop gain is decreased.

Consequently, the smart real time control input *u(t)* is a combination of a linear controllers augmented with the fuzzy tuned control parameters, such that ;

$$u = \frac{K_i+K_p \quad s+K_d s^2}{s} \tag{20}$$

4.0 SIMULATION AND PROTOTYPING OF PITCH ATTITUDE CONTROL

In this work, a two stage approach is used to develop and validate the smart SLV autopilot system. The first stage consists of two Hardware in the Loop simulations that are performed indoors. Part one of the first stage is a comparative analysis of the smart and classical gain selection schemes on the SLV autopilot systems under a nominally noisy condition.

In approach, the classical gains are derived based on Equations (10) - (13). Such that the transfer function of the PID feedback control loop for the deviation of the Pitch angle from the reference (θ_d) relative to the negative feedback input (θ_a) can be expressed as;

$$\frac{\theta_d(s)}{\theta_a(s)} = \frac{\left(k_p+k_d s+\frac{k_i}{s}\right)\left(\frac{k_1}{s^2-a_6}\right)}{1+\left(\frac{k_p s+k_d s^2+k_i}{s}\right)\left(\frac{k_1}{s^2-a_6}\right)} \tag{21}$$

Where, a_6 is the distributed aerodynamic moment due to angle of attack, and k_1 is the distributed moment due to the attitude control actuator. As a result, its corresponding characteristics equation in comparison with a normalized third order plant is given as;

$$s^3 + k_1 k_d s^2 - (a_6 - k_1 k_p)s + k_i k_1 = (s + 1/\tau)(s^2 + 2\zeta\omega_n s + \omega_n^2) \tag{22}$$

Selecting $a_6 = 3.2297$ and $k_1 = 7.0738$ as scaled from Ares I launch and flight parameters [19]. The gains are evaluated as follows;

$$k_p = \frac{2\alpha\varsigma\omega_n+{\omega_n}^2+a_6}{k_1};\ k_d = \frac{(2+\alpha)\varsigma\omega_n}{k_1};\ k_i = \frac{{\omega_n}^3\alpha\varsigma}{k_1} \tag{23}$$

such that, in frequency domain, the compact form of the control law is expressed as;

$$u = \frac{K_i+K_p \quad s+K_d s^2}{s} \tag{24}$$

In this case, it is important to note that k_1 and a_6 are scaled from the approximated rigid body dynamics of Ares I airframe. Consequently, the classical PID gains used for simulation at this stage are as shown in Table 1.

Table 1: Analytically determined PID gains

Gains	K_p	K_i	K_d
1	28.3	15	1.73
2	52.4	30	2.3
3	76.5	45.3	2.9
4	100.7	60.4	2.9
5	124.9	75.5	4.04

Figure 6: Photograph of the hardware in the loop experimental test rig

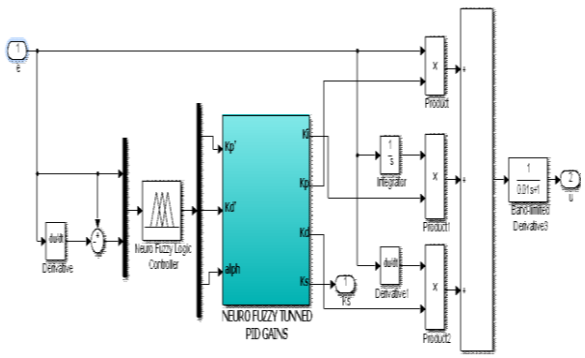

Figure 7: Simulink control scheme for the semi-intelligent pitch attitude control scheme

For the comparative analysis and feasibility test at this stage; the experimental set up consists of the miniaturized rocket that is shown in Figure 6. A 3-axis ITG320 is mounted on it. This is integrated into an arduino microprocessor on which the Simulink

control block in Figure 7 and classical PID gains that are computed in Table 1 are implemented apriori.

In this experiment, the vertical line is chosen as the reference axis on the pitch plane. A pitch attitude deviation of 16^0 was induced as step input in the presence of 5Km/h (fan induced) wind disturbance. The fan was located a meter away from the test rig. This disturbance was introduced to train the system to reliably handle the effects of sensor dynamics and atmospheric conditions. The picture of the experimental rig is as shown in Figure 6.

The time response of the classical and Fuzzy logic tuned PID control systems are compared in Figure 8. Whereas the smartly tuned PID controller presented a slightly more rippled transient response, its rise time and percentage overshoot are quite lower than that of the classical PID controller. The rippled initial response indicated the real time ability of the smart controller to handle structural oscillations of the slender airframe. Ultimately, the two controllers attained steady state simultaneously with approximately equal steady state errors. On the whole, it is shown that in situations where the classical controller is admissible; the Fuzzy tuned PID controller clearly gave improved performance and reliability.

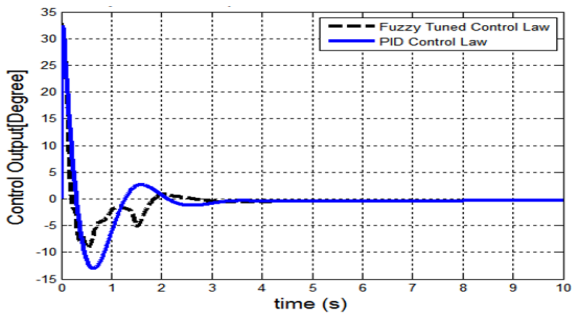

Figure 8: Comparative analysis of PID and smart fuzzy logic control schemes

4.1 Hardware in the Loop Prototyping for Control Algorithm Development

The first part of the indoor simulation on the HIL test rig established the feasibility of the smart SLV autopilot system. In preparation for its outdoor real time flight performance assessment, the second part of the indoor prototyping process is concerned with advancement of the smart control algorithm. This is to ensure high precision and robust performance in real flight conditions.

For this purpose, the experimental rig used at the earlier part of the indoor experiment is further equipped with complimentary hardware and sensors. The schematic layout of the enhanced experimental rig is as shown in Figure 9.

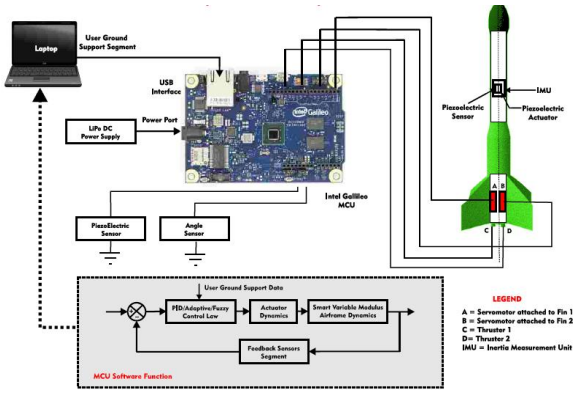

Figure 9: PID PC-Based hardware and software in the loop

In this case the fully developed experimental rig is as shown in Figure 9. It consists of four main units. These include the miniaturized flexible rocket that is embedded with a 3-axis ITG3200 gyroscope, a 3-axis ADXL345 accelerometer and a 3-axis HMR2300 smart digital magnetometer. This is in addition to embedded piezoelectric disc actuators that are used to induce structural vibrations. The second unit is made up of Arduino Intel Galileo Microcontroller interfaced with the flexible rocket and a personal computer. The servo motors, Simulink based control algorithm simulator interfaced to the Arduino Integrated development environment constitute the third unit.

To tune the Fuzzy logic based smart PID controller, the rocket is constrained to rotate in the pitch plane. It is actuated by fins and mono propellant thrusters. The actuator for the fins is a DC servo with 5V input voltage. Input to the thruster is also a 5V DC source. As described earlier, sensors on the rocket are for measurement of pitch plane acceleration, velocity and position in the pitch plane. Also, a dynamic piezoelectric disk sensor is mounted underneath the Inertia Measuring Unit (IMU) to continuously measure deflections of the airframe. On the whole, the control simulator replicates the rocket's behavior and trains the adaptive decision making scheme of the onboard soft controllers i.e. autopilot software for precision and robustness. As mentioned earlier, to ensure mission affordability, the overall system is based on open-source software and off-the-shelf hardware.

4.2 Real Time Flight Simulation for Autopilot Assessment

At the second stage of the autopilot prototyping scheme, the effectiveness of the smart algorithm is assessed through an outdoor real flight test. The flight

test bed shown in Figure 10 was configured for the demonstration and performance assessment. It is an on-board customized solid fuel research rocket initially designed for atmospheric probing. The tuned microcontroller, the sensors and IMU's used for prototyping in section 4.1 were integrated to the research rocket for real time in-flight data acquisition. This enables global positioning system (GPS) tracking of the rocket as well as transmission of its telemetry. The ensemble facilitates response analysis of the proposed non-rigid rocket pitch attitude control system.

Figure 10: The IMU Based autopilot flight module with GPS tracking station

For the real time flight test, a preplanned rocket trajectory of 700m altitude and 15 seconds flight duration was modelled for adaptive tracking such that the desired control objectives are assessed in real time through the onboard sensors and hardware. Thus, in-flight data logged by the accelerometer, gyroscope and magnetometer are shown in Figures 11, 12 and 13 represent the differences between the pre-planned values of the vertical acceleration, angular velocity and orientation in comparison with real time IMU measurements of the response of the controlled prototype rocket.

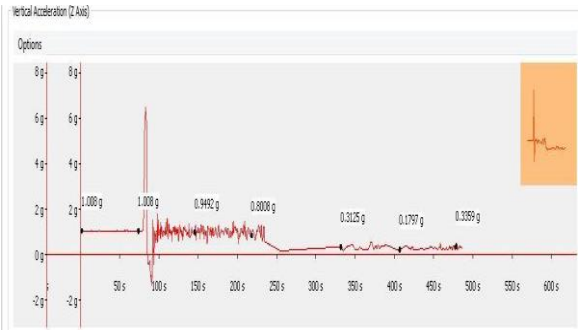

Figure 11: Vertical acceleration for research rocket trajectory as transmitted in flight from IMU

Relative to gravity (g), after the launch, the initial deviation of the rocket's vertical acceleration from referenced acceleration was recorded as 1.008g by the accelerometer. As regulated by the classical PID control scheme, this response steadied for about 87seconds into the flight duration. Subsequently, strong interference between the oscillation of the slender airframe and onboard instrumentation hardware shot the system beyond the control bandwidth of analytically selected PID gains. Hence, the accelerometer reading fluctuated widely between 6.2g and -1.8g within 7 seconds of the flight duration. Thus, the reference is overshot by 496.23%.

To regulate the sharp deviation from the referenced acceleration value, the fuzzy logic based gain selection process is triggered. Apparently, the smart controller attenuated the transient vertical acceleration deviation to 0.8008g in 140 seconds. Thereafter, the acceleration steadied to an error of less than 0.002g of the reference acceleration for the rest of the flight. The time response of the vertical acceleration variation due to initial jerk from the thruster as measured by the ADXL345 accelerometer is presented in Figure 11.

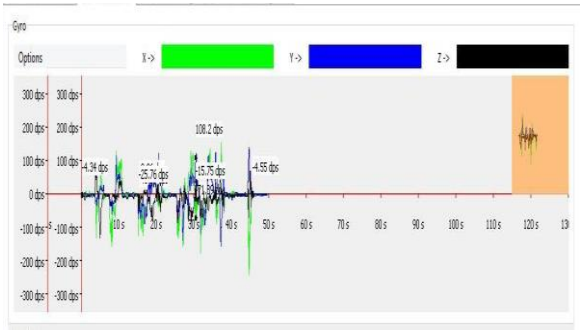

Figure 12**:** Gyro output for research rocket trajectory as transmitted in flight from IMU

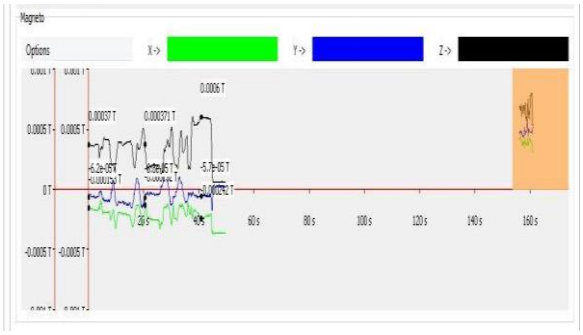

Figure 13: Magnetometer output for research rocket trajectory as transmitted in flight

Similarly, the 3-axis ITG3200 gyroscope tracked the controlled response of deviations of the angular velocities of protoyped rocket along the x, y and z axes. In comparison with the referenced profile; as

expected, due to the gimbal effect of the thruster, the deviation dynamics of the angular velocity is much pronounced on the x-y plane. This is in addition to a much more faster response that peaked serially with increasing amplitudes and bandwidths about six times within 45seconds of the launch. However, the 216.4dps variation of bandwidth at 45seconds switched the PID gains selection module from classical to intelligent mode. Consequently, the transients settled in less than 5seconds with near zero steady state error.

In Figure 13, magnetic field variations along the *x*, *y* and *z* axes relative to the set references are recorded by the onboard HMR2300 smart digital magneto-meter. Unlike the 15seconds and 5seconds time delay that were observed for the accelerometer and gyroscope, respectively, the magnetomer response was delayed for 7seconds in all directions. As expected, magnetic field variation that indexed the relative altitude of the launch vehicle to the launch pad is most pronounced on the vertical (z) axis. In comparison to its initial value of 3.7 Gauss along the z axis prior to the launch, the variation recorded 11 peaks within the first 42 seconds of the flight trajectory. The amplitudes of these peaks ranged between 3.708 Gauss to 6.02 Gauss within this period. These sharp variations indexed poor ability of the classical PID regulator to cancel out the effect of airframe oscillation from magnetometer instrument-ation data. Subsequently, switching to smart PID gains selection damped and steadied the measured magnetic field variation along the z axis to 0.02 Gauss in less than 5 seconds.

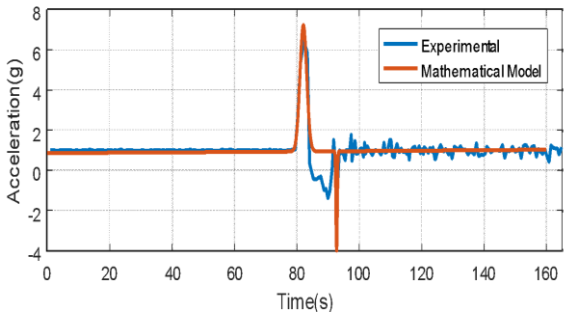

Figure 14: Z-axis accelerometer measurement

To validate the reliability of the hybrid pitch attitude control system and its development environment; the real time variation of the inflight accelerometer readings along the (vertical) z – axis is numerically compared with the reference values on the pre-planned trajectory. As shown in Figure 14, apart from the sharp variation in the expected measurement that occurred at the turning point i.e. midway into the flight duration, the smart regulator adapted the response variation to approximately 2% of the reference value. However, in this case, the switch between analytical and inteligent gain selection modes was triggered midway into the flight duration. On the whole, there is an approximate 97.8% convergence between the accelerometer readings and experimental values. This validates the reliability of the developed scheme.

5.0 CONCLUSION

Using simulation and experimental approach, this work illustrated the effects of airframe oscillation on the precision of onboard instrumentation and control hardware on slender microsatellite launch vehicles. It demonstrated the potential of hybrid (analytical and intelligent) PID gains computing algorithms for adaptive decision making on the pitch attitude control system. In essence, a computational framework has been developed for smart tuning of control parameters to regulate the effects of system's nonlinearities such as time delay, oscillatory error feedback on the model reference adaptive control pitch attitude autopilot loop. In general, a new environment for developing and validating smart controllers that estimate non linear effects of plant dynamics resulting from structural vibrations for real time decision making has been facilitated. Convergence of experimental and theoretical results established the reliability of the developed tool.

REFERENCES

[1] National Security Technology Accelerator, "Reducing the Cost of Space Travel with Reusable Launch Vehicles," https://nstxl.org/reducing-the-cost-of-space-travel-with-reusable-launch-vehicles, 2024.

[2] M. Trikha, M. D. Roy, S. Gopalakrishnan and R. Pandiyan, "Structural stability of slender aerospace vehicles: Part II: Num-erical simulations," *International Journal of Mechanical Sciences*, vol. 52, no. 9, pp. 1145-1157, 2010.

[3] A. L. Greensite, Analysis and Design of Space Vehicle Flight Control Systems, vol. VII, General Dynamics Corporation, 1967.

[4] S. Khadem and J. Euler, "Dynamic stability of flexible spinning missiles. II-Vibration and stability analysis of a structurally damped controlled free-free Bernoulli-Euler beam, as a model for flexible missiles.," in *33rd Structures, Structural Dynamics and Materials Conference*, 1992.

[5] H. D. Choi and H. and Bang, "An adaptive control approach to the attitude control of a

flexible rocket," *Control engineering practice*, vol. 9, no. 8, pp. 1003-1010, 2000.

[6] W. Du, Dynamic modeling and ascent flight control of Ares-I Crew Launch Vehicle, Ames, Iowa: Iowa State University ProQuest Dissertations Publishing, 2010, p. 24.

[7] L. Minjiao, R. Xiaoting and K. A. Laith, "Elastic Dynamic Effects on the Trajectory of a Flexible Launch Vehicle," *Journal of Spacecraft and Rockets*, vol. 52, no. 6, 2015.

[8] G. Kerschen, M. Peeters, J. C. Golinval and C. Stéphan, "Nonlinear modal analysis of a full-scale aircraft," *Journal of Aircraft*, vol. 50, no. 5, pp. 1409-1419, 2013.

[9] M. R. Eressa, Z. Danchen and H. Min, "PID and neural net controller performance comparsion in UAV pitch attitude control," in *2016 IEEE International Conference on Systems, Man, and Cybernetics (SMC)*, Budapest, Hungary, 2016.

[10] J. Jiann-Woei, A. Abran, H. Robert, B. Nazerth, H. Charles, R. Stephen and J. Mark, "Ares I Flight Control System Design," in *AIAA Guidance, Navigation, and Control Conference*, Toronto, Ontario Canada, 2010.

[11] T. A. Fashanu, L. M. Adetoro, O. S. Asaolu and A. A. Ayorinde, "A Cross Reference Analysis of Adaptive Piezoelectric Actuator Reinforced Slender Airframes for Microsatellite Launch Vehicles," *Journal of Engineering Research*, vol. 27, no. 3, pp. 11-25, 2022.

[12] Y. Zhu, X. Huang, W. Fang and S. Li, "Trajectory Planning Algorithm Based on Quaternion for 6-DOF Aircraft Wing Automatic Position and Pose Adjustment Method," *Chinese Journal of Aeronautics*, vol. 23, no. 6, pp. 707-714, 2010.

[13] N. V. Kadam, "Practical Design of Flight Control Systems: Some Problems and Their Solutions," *Defence Science Journal*, vol. 55, no. 3, pp. 211 – 221, 2005.

[14] B. Maurizio, "VEGA Missionization and Post Flight Analyses," 2009.

[15] O. Ibidapo-Obe and A. B. Sofoluwe, "A note on stability of some parametrically excited structural elastic systems," *Applied Mathematical Modelling*, vol. 6, no. 3, pp. 202-204, 1982.

[16] X. Yu, Y. Fu and Y. Zhang, "Aircraft Fault Accommodation With Consideration of Actuator Control Authority and Gyro Availability," *IEEE Transactions on Control Systems Technology*, vol. 26, no. 4, pp. 1285-1299, 2018.

[17] R. K. Kincaid and P. Sharon L, "D-optimal designs for sensor and actuator locations," *Computers and Operations Research*, vol. 29, no. 6, pp. 701-713, 2002.

[18] Y. Bar-Shalom, X. Li, T. Kirubarajan, "Estimation with Applications to Tracking and Navigation: Theory, Algorithms and Software: State Estimation for Nonlinear Dynamic Systems" *John Wiley and Sons, Inc.* pp. 371-420, 2002.

[19] D. B. Ralph, D. T. Justin, C. R. Mercedes, G. H. Lucas, L. G. James, A. B. Paul, A. P. Russell and R. L. Daniel, "Ares I-X Launch Vehicle Modal Test Overview," in *Society for Experimental Mechanics Series*, New York, 2011.